



Contents lists available at ScienceDirect

Environmental Pollution

journal homepage: www.elsevier.com/locate/envpol

Metal availability in a highly contaminated, dredged-sediment disposal site: Field measurements and geochemical modeling

Julie Lions^{a,e,*}, Valérie Guérin^{a,e}, Philippe Bataillard^{a,e}, Jan van der Lee^b, Agnès Laboudigue^{c,d,e}

^a BRGM, 3 Avenue Claude Guillemin, 45060 Orléans Cedex 2, France

^b Mines ParisTech, Centre de Géosciences, 77305 Fontainebleau Cedex, France

^c Univ Lille Nord de France, F-59000 Lille, France

^d EMDouai, MPE-GCE, F-59500 Douai, France

^e Centre National de Recherche sur les Sites et Sols Pollués, BP 537, 59505 Douai cedex, France

A detailed case study of metal behavior in a dredged-sediment disposal site combined with geochemical modeling.

ARTICLE INFO

Article history:

Received 1 September 2009

Received in revised form

27 May 2010

Accepted 12 June 2010

Keywords:

Dredged sediment

Metal

Arsenic

Geochemical modeling

Leaching

ABSTRACT

Two complementary approaches were used to characterize arsenic and metal mobilizations from a dredged-sediment disposal site: a detailed field study combined with hydrogeochemical modeling. Contaminants in sediments were found to be mainly present as sulfides subject to oxidation. Secondary phases (carbonates, sulfates, (hydr)oxides) were also observed. Oxidative processes occurred at different rates depending on physicochemical conditions and contaminant contents in the sediment. Two distinct areas were identified on the site, each corresponding to a specific contaminant mobility behavior. In a reducing area, Fe and As were highly soluble and illustrated anoxic behavior. In well-oxygenated material, groundwater was highly contaminated in Zn, Cd and Pb. A third zone in which sediments and groundwater were less contaminated was also characterized. This study enabled us to prioritize remediation work, which should aim to limit infiltration and long-term environmental impact.

© 2010 Elsevier Ltd. All rights reserved.

1. Introduction

Dredged sediments have been disposed on river banks for decades, creating environmental hazards in industrial areas where effluents have contaminated sediments. In sediments, inorganic contaminants such as As, Zn, Cd, Pb, Se, Ni are often in thermodynamic equilibrium under reducing conditions, and are generally associated with sulfide mineral phases. Exposing the sediments to air leads to progressive oxidation of these phases and the subsequent solubilization of the associated contaminants. The elements thus released can either precipitate as secondary phases (sulfates, phosphates, hydroxides), remain in solution or be retained by hydroxides, clays and organic matter (Calmano et al., 1993; Tack et al., 1996; Gabler, 1997; Cauwenberg and Maes, 1997; Du Laing et al., 2009). The redistributed contaminants are potentially more mobile than the original reduced sulfide form (Tack et al., 1996; King et al., 2006; Hartley and Dickinson, 2010). Despite the occasionally strong buffer capacity of sediments, pH also plays a role in releasing metal (Calmano et al., 1993). The significant role of calcium on the mobilization process has also been reported

(Christensen, 1984; Wang et al., 1997; Lions et al., 2007). Given the complexity of the system, the mobility of inorganic pollutants is difficult to predict and to manage.

In order to better understand the metal behavior, we carried out a detailed field study of an old dredged-sediment disposal site highly contaminated with metals and arsenic, and combined this with geochemical modeling. In spite of the vast number of geochemical processes potentially involved, we hoped that geochemical modeling would provide insight into the mechanisms involved in contaminant mobility and possible explanations for field observations.

2. Materials and methods

2.1. Site description

The site studied is a thirty-year-old dredged-sediment disposal site in the North of France, on the banks of the Haute-Deûle canal (Fig. 1), near metallurgical plants. The canal water and bottom sediments have been the receptacle of large amounts of heavy metals (Bourg et al., 1989). The underlying bedrock is the Senonian chalk that constitutes the major regional aquifer. This aquifer formation is covered by about 5 m of undisturbed Quaternary alluvium and there are clay aquitards in the northern part of the site. The disposal site covers 6 ha and the 2–4 m thick layer of dredged-sediments deposited aboveground is not in contact with the groundwater.

Successive dredging operations have created a complex disposal site composed of numerous layers with different compositions and textures. The site opened in

* Corresponding author.

E-mail address: j.lions@brgm.fr (J. Lions).

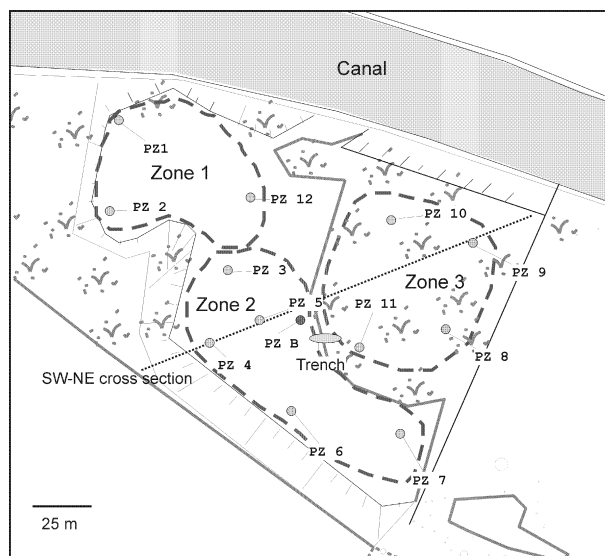


Fig. 1. Canal sludge disposal site and location of sampling points in Zone 1 (hydromorphic), Zone 2 (well-oxygenated sediment) and Zone 3 (weakly contaminated sediment).

1969 with the deposition of an initial layer of uncontaminated sludge and fill embankments were erected. In 1972, the canal was deepened and 20 000 m³ of sediments, alluvium and probably chalk were added. Between 1972 and 1975, soil developed on top of the sediments. The top layer of sludge (~26 000 m³) was deposited in 1976. This material comes from the canal terminal basin of a nearby Pb–Zn smelting plant and is highly contaminated. There is no vegetation on part of the site due to the high concentration of contaminants.

2.2. Sampling and sediment analysis

A surface sediment profile was obtained from a trench 1 m deep in an area with no vegetation (Fig. 1). Twelve boreholes were drilled and sediment samples were collected at regular intervals between 20 cm and down to 3 m below ground level (mbgl), wherever possible. One deeper well (PZB) was drilled down to the regional chalk formation (12 m). Solid samples were dried at 40 °C and 57 visually distinguishable (color, texture) samples were selected for analyses. Grain size distributions were determined using the pipette method (AFNOR X31-107). Total and inorganic carbon contents were measured on crushed sediment samples with a total organic analyzer (TOC-5000A, Shimadzu) equipped with a solid sample module. Total concentrations of major and trace elements were determined in triplicate by plasma atomic emission spectrometry (ICP-AES, Jobin-Yvon 138) after microwave-assisted acid digestion according to the aqua regia method NF X33-010 (AFNOR). The major mineralogical phases were identified on powder samples by X-ray diffraction (XRD) (Panalytical X'PERT PRO).

2.3. Water sampling and monitoring

Perched aquifers 50 cm to 2–3 m deep were monitored in wells PZ1 to PZ12 (Fig. 2). Water levels were recorded weekly over an 18-month period and groundwater samples were collected twice a month. Monitoring in some wells was interrupted when the water level dropped below the well screen.

Temperature, pH, Eh and conductivity were measured in situ at each sampling point using a multi-parameter water-quality monitoring instrument (Aqualyse, Memodat 4). Groundwater was collected by pumping (GIGANT 9 L/min), without preliminary well purging because of the low permeability of the sediments (some wells needed more than 2 days to reach hydraulic equilibrium). To ensure that Eh was not overestimated, the effect of purging was tested on several wells and showed that even without purging, the water was not in equilibrium with atmospheric oxygen.

2.4. Water analyses

Water samples were filtered at 0.45 µm (acetate cellulose filters). One fraction of each sample was analyzed immediately for anions and carbon content, and another was acidified with 2% HNO₃ and stored at 4 °C for subsequent major and trace element analyses. Dissolved organic and inorganic carbon were measured with a TOC analyzer (Shimadzu-TOC 5000). Anions were quantified by ionic chromatography (Dionex 500). Major and trace elements were determined by ICP-AES (Jobin-Yvon 138).

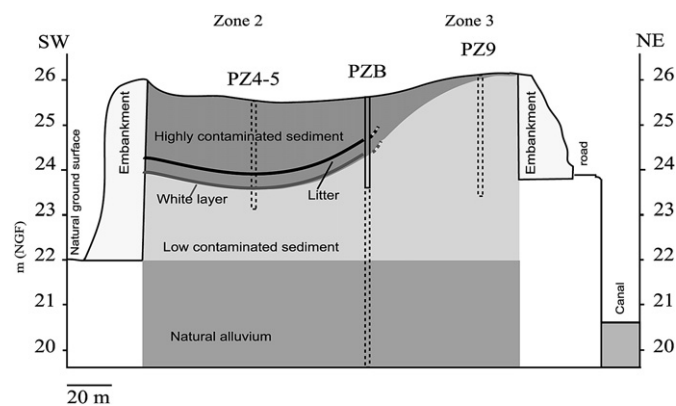


Fig. 2. Structure of the deposit – SW–NE cross section (see Fig. 1).

2.5. Geochemical model

Geochemical modeling was done using the physicochemical parameter data from the wells, assuming thermodynamic equilibrium, to characterize the processes and parameters that control arsenic and metal availability. The reaction paths calculated by the model must, therefore, be interpreted carefully, keeping in mind that no kinetics were taken into account and that only the minerals defined in the database are likely to precipitate. In the field, the most likely controlling phases—those that are the most soluble and precipitate easily—are usually amorphous phases. Nevertheless, modeling can help in supporting research hypotheses.

Geochemical modeling was done with the CHESSE code using the CHESSE database (Van der Lee, 1998), based on the LLNL (EQ3/6) thermodynamic dataset. Reaction pathways for simplified geochemical systems took into account the minerals and physicochemical conditions of the system (pH, CO₂, Eh). The influence of organic matter and clay sorption processes were not taken into consideration in this model because metals were so abundant that they were controlled mainly by mineral solubility.

Three simulations were done to study contaminant mobility. For each simulation, the thermodynamic equilibrium was calculated for a unique mineralogical assemblage representative of the initial dredged sediment for a redox potential range (PZ1 and PZ2 simulations) or a pH range (PZ4 simulation). The sediment model with relevant phases was composed of calcite, quartz and a suite of sulfides: pyrite, sphalerite (ZnS), galena (PbS) and greenockite (CdS). The mineralogical assemblage was equilibrated with water, using an initial CO₂ fugacity of 0.038 atm, a pH of 6.7 for simulation PZ1, and a pH of 7.2 for simulation PZ2 to reproduce PZ1 and PZ2 conditions respectively. The reaction pathways and aqueous speciations were calculated for Eh values ranging from –0.3–0 V. In simulation PZ4, the mineralogical assemblage was equilibrated under oxidizing conditions (Eh at 0.3 V), with a pCO₂ at 0.017 atm. Due to the observed pH variability and the dependency of carbonate solubility, a pH range of 5.5–7.5 was used in the model in order to reproduce the range observed in PZ4 to PZ11.

3. Results

3.1. Sediment characteristics

3.1.1. Field investigations

Four layers could be distinguished in the trench (Table 1). The top layer (T), 50 cm thick, is composed of grey silty–loam. It contains mud–cracks, probably caused by climate variations in the absence of vegetation. Large cracks are filled with a coarser material

Table 1

Grain size distribution of selected samples from the sediment trench (fraction in %).

Depth (cm)	Top layer sediment (T)		Under litter sediment (M)		White layer (W)
	Cracks	Matrix	Upper	Lower	
	0–50	0–50	50–65	65–70	80–85
Clay (<2 µm)	17.4	18.2	20.8	35.8	34.4
Fine silt (2/20 µm)	52.4	59.8	13.8	25.5	53.4
Coarse silt (20/50 µm)	20.5	20.4	18.5	20.8	5.3
Fine sand (50/200 µm)	5.6	1.5	46.3	17.6	2.9
Coarse sand (200/2000 µm)	4.1	0.1	0.6	0.3	4.0

(10% sand vs. 1.5% in the matrix) that probably facilitates gaseous exchange with the atmosphere and preferential water flow. Red coatings, characteristic of ferrous oxides/hydroxides, which precipitate in contact with oxygen, are visible along the cracks. Layer T overlies a layer of ground litter (L) composed of organic matter (roots, leaves) that is only slightly decomposed, even after 30 years. Layer L overlies a 10–20 cm-thick layer (M) that can be further divided into two sub-layers according to texture; silty-clay loam at the bottom and loam at the top. The litter shows that several years passed between the deposition of layers T and M, during which vegetation developed. Under these layers, there is a layer of white silty-clay loam (W), 5–10 cm thick, overlaying another layer of sediment.

Boreholes enabled us to determine the lateral and vertical extent of the sediment layers in the disposal site (Fig. 2). In PZ1 to PZ3 and PZ12, the texture and smell of a viscous black sediment (B), 1–2 m deep, reveals the presence of hydrocarbons. Between 0 and 1 m, these characteristics are not observed due either to alteration or to the fact that the black sediment has been overlain by a brownish sediment similar to the material in layer T observed in the trench. In PZ4 to PZ7, like in the trench, sediment T is observed at the top and the litter L is encountered about 0.7–1.6 mbgl, overlaying a brownish sediment layer M. The white layer W is encountered between 1.3 and 2 mbgl. Below this, a grey-blue-colored sediment (GB) is clearly visible. In PZ8 and PZ9, there is a brownish sediment down to a depth of 1 m, overlaying the grey-blue sediment GB. In PZ10, a thin surface layer of sediment, 20 cm thick, overlies a layer composed mainly of backfill (down to a depth of 1.5 m), below which the grey-blue sediment GB is visible.

3.1.2. Total element concentrations

Major element concentrations (Ca, Mg, K, Al, Fe) are relatively homogeneous (Table 2) throughout the disposal site, except in the white layer W, which contains large amounts of calcium due to its mineral composition (mainly calcite). In reality, all Deûle River sediments have a similar composition, which is controlled by the regional geology. This has also been observed for titanium and nickel concentrations, which have a geological origin (Vallee, 1999). In contrast, there is a large vertical variability in Cd, Pb, Zn and As concentrations that is related to the sediment deposition history. Three levels of contamination ranging from very high to low could be differentiated in the 57 samples (Table 3). Regardless of the level of contamination, there is a close correlation between these metals (R^2 : As/Pb: 0.78; Zn/Pb: 0.9; Zn/Cd: 0.72), which indicates a consistent association of these elements in the sources. Furthermore, weakly contaminated layers have metal contents higher than the regional soil values for Zn (55 mg kg⁻¹), Pb (18 mg kg⁻¹) and Cd (0.12 mg kg⁻¹) (Darmendrail et al., 2000).

Fig. 3 shows the vertical distribution of lead and arsenic in 3 different wells representative of groups of wells with similar

Table 2

Major element concentrations (mg/kg dry matter) in sediment samples between 0 and 3 m deep (57 samples).

mg/kg	Median	Mean \pm SD	Max	Min
Mg	7729	8700 \pm 3192	14 561	3882
Ca	44 908	53 762 \pm 24 330	150 833	19 231
Al	30 346	34 614 \pm 15 007	59 524	15 150
Na	541	588 \pm 166	978	208
K	7998	10 113 \pm 5037	18 247	3435
Ni	26	26 \pm 7	48	17
Mn	186	204 \pm 104	699	85
Ti	848	838 \pm 141	1096	404
Fe	33 710	32 196 \pm 7990	48 983	11 123

Table 3

Metal and As concentrations (mg/kg dry matter) among the three levels of contaminated sediments between 0 and 3 m deep (57 samples).

mg/kg		Median	Mean \pm SD	Max	Min
As	H	3157	3684 \pm 2103	8051	550
	M	93	133 \pm 113	392	6
	L	8	9 \pm 5	16	5
Zn	H	38 033	39 479 \pm 19 112	83 422	11 367
	M	3419	3247 \pm 1355	6775	1148
	L	342	349 \pm 163	683	177
Cd	H	3131	3506 \pm 2018	7893	759
	M	238	466 \pm 437	1431	35
	L	0	1 \pm 2	4	0
Pb	H	66 347	60 115 \pm 26 132	105 510	8916
	M	1472	1729 \pm 1272	4828	124
	L	70	100 \pm 61	222	47

H: high contamination; M: medium contamination; L: low contamination.

sediment layers. The highest level of contamination is observed in layer T, around 0.5 m deep in PZ1 and between 0 and 1.2 m deep in PZ6. In PZ1, the black sediment layer B below layer T is also contaminated (from 1 to 2 m deep), but to a lesser extent. In PZ6, below the litter layer L, As, Zn, Cd and Pb concentrations rapidly decreased in the profiles to levels of no environmental concern in the GB layer. In PZ8 to PZ11, located in the area with vegetation, only the thin surface layer is contaminated. These highly-contaminated materials match the sediments from the canal terminal basin that were deposited in 1976.

The total organic carbon (TOC) content in layer T (0–50 cm) ranges from 6 to 8%. In layers 50–100 cm deep, TOC values are between 3 and 6%, and below 100 cm they were between 0.1 and 3%. The black layer contains a large amount of organic matter (TOC ranging from 5 to 11%).

3.1.3. XRD characterization

The major minerals identified by XRD in the sediments were quartz, calcite and clays. Feldspar, pyrite, plagioclase and dolomite are also present. In surface samples (down to 1 m), gypsum was identified as a product of sulfide oxidation. The ferrous precipitates visually observed were not identified by XRD, possibly due to their amorphous structure. Goethite was characterized in trench sample as a result of meticulous sampling (Lions, 2004). XRD analyses of samples from three profiles (PZ1, PZ3 and PZ4) and the trench

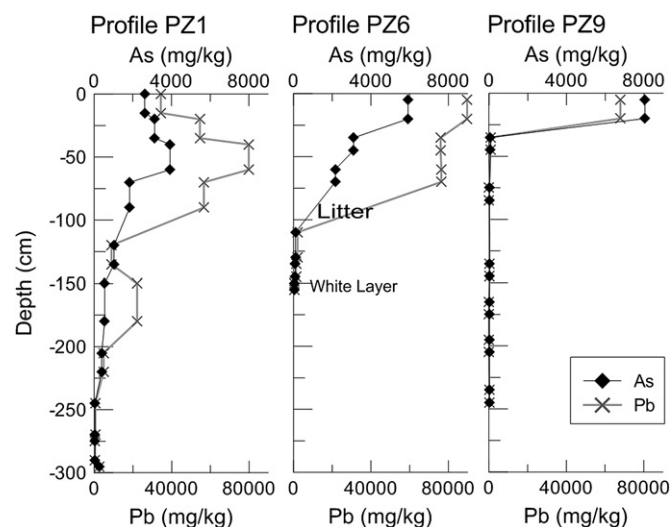


Fig. 3. Lead and arsenic concentrations in sediments vs. depth (mg/kg) along 3 profiles (PZ1, PZ6, PZ9).

Table 4
Mean pH and conductivity of water samples from the 12 wells.

		Number of samples	pH			Cond (mS/cm)
			Mean \pm SD	Min	Max	Mean \pm SD
Zone 1	PZ1	23	6.7 \pm 0.2	6.2	7.1	2.3 \pm 0.3
	PZ2	23	7.2 \pm 0.3	6.7	7.8	2.6 \pm 0.1
	PZ12	10	6.7 \pm 0.25	6.4	7.3	3.0 \pm 0.3
Zone 2	PZ3	8	6.4 \pm 0.15	6.2	6.7	3.7 \pm 0.2
	PZ4	23	6.0 \pm 0.3	5.5	6.5	3.2 \pm 0.1
	PZ5	23	6.2 \pm 0.26	5.7	6.7	2.9 \pm 0.4
	PZ6	23	6.3 \pm 0.4	5.7	6.9	2.5 \pm 0.6
	PZ7	23	6.2 \pm 0.35	5.6	6.8	2.5 \pm 0.2
Zone 3	PZ8	2	6.8 \pm 0.05	6.7	6.8	2.6 \pm 0.1
	PZ9	12	6.5 \pm 0.5	6.1	7.1	2.6 \pm 0.4
	PZ10	9	6.4 \pm 0.4	5.8	6.8	2.9 \pm 0.1
	PZ11	4	6.6 \pm 0.1	6.5	6.6	3.1 \pm 0.1

revealed the presence of sphalerite and galena (PbS) in the most contaminated layers. The presence of galena as the principal lead-bearing mineral throughout the profile is likely related to the stability of this phase in reducing sediments. Anglesite (PbSO₄) was identified in samples from the trench along cracks. Cerussite (PbCO₃) was observed throughout the contaminated profiles, but the content decreases progressively with depth.

3.2. Disposal site structure

We were able to distinguish three zones in the disposal site (Fig. 1). Zone 1, around PZ1 and PZ2 and some of PZ12, is characterized by the viscous, black sediments from layer B that contain hydrocarbons. Zone 2, encompassing PZ3 to PZ7 and some of PZ12, is characterized by sediments T corresponding to the profile observed in the trench. PZ3 is transitional between Zones 1 and 2. While layers B and T are both made up of heavily contaminated sediments, layer B also contains hydrocarbons, which modify mechanical and hydrochemical properties and have led, in the 30 years since they were deposited, to two different evolutionary processes: hydromorphy in Zone 1 and the formation of a cracked surface layer in Zone 2. There is no vegetation in either zone. A third zone, Zone 3, encompassing PZ8 to PZ11, is characterized by weakly contaminated sediment

covered by a thin, surface layer (10–30 cm) of highly-contaminated material. This is the only zone where there is vegetation.

3.3. Groundwater

3.3.1. Water tables

Groundwater was observed at a depth of between 0.5 and 2 m in wells PZ1 to PZ12, whereas the deposit is unsaturated between 3 and 5 m bgl. Perched aquifers are not unexpected in this type of system due to the differences in permeability of the various layers. No seepage has been observed through the embankments around the disposal site, hence there is no lateral flow leaving the site. Flow is apparently predominantly downward.

In PZ1 and PZ2, water level variations caused by heavy rainfall are delayed compared to those in the other wells. In this area, the permeability is low due to the high hydrocarbon content and, therefore, viscous texture of the sediments. Water levels in PZ1 and PZ2 were different, indicating there might be several distinct perched aquifers in this area.

In PZ3 to PZ7, the water level rose rapidly after rainfall. Permeability is higher here than in Zone 1 and open cracks create preferential pathways. During the winter, the water levels were the same in all the wells, indicating hydraulic continuity. Water levels never dropped below the level of layer W (23.5 or 24 m), which might retain perched groundwater during phreatic lows. This layer is absent in PZ1 and PZ2, but the year-long retention of groundwater in Zone 1 might be explained by the low permeability of the viscous black sediments. PZ3 and PZ12 were damaged during the monitoring campaign and the data they furnished are incomplete.

The water levels in wells PZ8 to PZ11 and their drainage rates between March and July were similar. The wells did not reach the water table (>3 m deep) in the summer and autumn due to low recharge. The stratification of the disposal site in this area explains the absence of permanent perched aquifers. The sediments have a coarser texture, the white layer W is not present and there is some vegetation, which enables efficient evapo-transpiration. The permeability is higher here, as confirmed by the rapid renewal of water in the wells after purging. Hydrological trends in PZ11 are intermediate due to its location. In situ Lefranc trials done in the deep well (PZB, Fig. 1) indicate a permeability of 2.6×10^{-6} m/s

Table 5
Water composition of the 12 wells: major cations, anions and DOC. Concentrations in mg/L (mean \pm SD).

		DOC	HCO ₃ ⁻	Cl ⁻	SO ₄ ²⁻	Mg	Ca	Na	K	Si	P
PZ 1	mean	72.6	1867	12.41	138.3	48.6	420.3	15.07	22.98	17.49	0.225
	SD	75.5	455	3.25	119.7	5.2	75.7	5.57	2.22	1.61	0.287
PZ 2	mean	17.0	702	9.89	1098	83.7	493.5	17.87	58.29	6.02	0.057
	SD	15.2	136	2.06	89.8	5.5	41.1	7.27	3.51	0.56	0.031
PZ 3	mean	10.1	141.8	10.65	3138	120.9	543.5	19.91	71.70	8.60	0.031
	SD	1.4	65.5	2.83	726.7	8.0	36.9	11.67	2.95	1.58	0.010
PZ 4	mean	8.8	47.9	10.45	2315	28.8	550.6	3.27	28.85	8.93	0.027
	SD	1.7	18.4	8.26	165.4	4.9	33.8	1.56	2.47	1.34	0.012
PZ 5	mean	10.0	71.2	5.80	1896	41.0	537.3	3.95	32.28	7.88	0.027
	SD	4.8	29.4	1.30	297.5	4.9	44.1	1.69	2.35	1.54	0.011
PZ 6	mean	9.9	51.3	7.33	1583	24.7	487.3	2.70	23.81	5.68	0.022
	SD	9.1	19.7	3.02	448.6	10.2	87.4	2.03	5.43	2.27	0.009
PZ 7	mean	8.1	143.4	6.81	1509	28.6	524.7	4.80	17.41	6.66	0.024
	SD	9.2	85.2	2.58	155.3	13.5	76.8	4.99	1.36	0.72	0.010
PZ 8	mean	31.1	548	12.55	2843	68.0	614.0	11.12	15.64	7.31	0.017
	SD	27.9	43.5	0.92	78.5	4.5	25.5	1.44	0.42	0.14	0.001
PZ 9	mean	9.5	558	9.18	1070	65.9	594.4	10.42	11.75	8.38	0.252
	SD	9.9	290	2.32	210	15.4	121.4	7.81	3.82	0.57	0.309
PZ 10	mean	3.7	910	24.27	1782	89.8	696.1	23.14	21.22	7.81	0.019
	SD	3.4	221	2.76	749	7.9	33.8	6.88	2.27	1.04	0.014
PZ 11	mean	2.9	716	33.15	2357	102.2	633.3	41.90	20.83	7.68	0.022
	SD	1.2	87.5	8.96	896	7.5	15.7	14.71	2.92	1.91	0.014
PZ 12	mean	20.0	453	16.46	1507	68.0	591.0	27.83	28.47	7.16	0.025
	SD	15.5	89.1	8.22	387	26.6	87.0	10.83	15.68	2.14	0.020

between 22 and 23 mbgl, which is that of fine sand and sandy loam. A permanent perched water table would require a layer of lower permeability (Lions, 2004).

3.3.2. Groundwater geochemistry

Mean values for chemical parameters and aqueous concentrations were highly variable (Tables 4–6, for all data see Lions, 2004). The hydrochemical facies, as plotted on a Piper diagram (Fig. 4), show that groundwater composition is specific to its location. PZ1 groundwater is of the calcium–bicarbonate type, whereas groundwaters in PZ2 and PZ8 to PZ12 are of the calcium–sulfate type. PZ3 to PZ7 groundwaters are of the hyper-sulfate type often associated with gypsum-bearing aquifer formations and groundwater affected by sulfide mineral oxidation.

PZ1, PZ2 and PZ12 contain water with pH values above 6.7 and redox potentials for the most part below 0.2 V/ENH, although the redox measurements are slightly overestimated due to the sampling protocol (under atmospheric conditions). The PZ1 water has a high dissolved organic carbon content. The waters in PZ1 and PZ2 have high iron concentrations ($0.5\text{--}9.5\text{ mg L}^{-1}$), probably mainly as Fe(II) and arsenic ($0.45\text{--}4.8\text{ mg L}^{-1}$), while Zn, Cd and Pb concentrations were relatively low.

PZ3 to PZ7 contained acidic waters with a mean pH below 6.5 and minimum values of 5.5 associated with high redox potentials ($>0.3\text{ V/ENH}$). Some conductivity values are higher in this zone due to greater mineralization. The waters have high sulfate concentrations (means from $1.5\text{ to }3.1\text{ g L}^{-1}$) and are highly contaminated in Zn (up to 846 mg L^{-1}), Cd (up to 138 mg L^{-1}), Mn (up to 8.3 mg L^{-1}) and Pb (up to 4.79 mg L^{-1}). Fe and As concentrations are low compared to those found in PZ1 and PZ2.

Although the physicochemical parameter values for PZ8 to PZ11 fall between those observed in the other wells, the chemical compositions of these groundwaters distinguish them from the others. They contain much less Zn, Cd and Pb than waters from PZ3 to PZ7, but more carbonates. PZ8 and PZ11 waters were the most highly-concentrated in this zone and might be slightly contaminated by lateral inflow of nearby highly-contaminated groundwater. Due to its reducing properties, probably related to the

relative depth of the well, the groundwater in PZ9 contains higher Fe and Mn concentrations.

The aqueous concentrations measured for Zn, Cd, Pb, As and Fe were plotted on log-scale graphs (Fig. 5) confirming the 3 distinct water-quality groups. PZ3 to PZ7 waters are highly contaminated in Zn, Pb and Cd. PZ1, PZ2 and PZ12 contain high concentrations of Fe and As. PZ9 falls between these two groups. PZ8 to PZ11 also contain metals and arsenic but concentrations are never as high as those observed in the others wells.

3.4. Geochemical modeling

There are many limitations to thermodynamic modeling of such complex systems. The very sharp changes as a function of redox potentials that are calculated with models are not likely to be observed in the field. This is because many redox processes tend to be slow or are catalyzed by microorganisms. A geochemical model

Table 6

Water composition of the 12 wells: main metals and arsenic. Concentrations in mg/L (mean \pm SD) and drinking water guidelines (WHO).

		As	Zn	Cd	Pb	Ni	Mn	Fe
PZ1	mean	0.455	0.193	0.002	0.007	0.004	1.07	9.41
	SD	0.357	0.216	0.002	0.004	0.002	0.29	5.57
PZ2	mean	4.80	3.9	0.021	0.065	0.007	0.84	0.54
	SD	4.47	2.3	0.038	0.071	0.004	0.18	1.79
PZ3	mean	0.023	567.0	41.2	1.36	0.194	6.20	0.024
	SD	0.005	218.5	25.1	0.511	0.069	1.46	0.016
PZ4	mean	0.011	687.6	113.2	3.46	0.197	4.24	0.058
	SD	0.007	72.2	14.2	0.863	0.046	1.13	0.050
PZ 5	mean	0.026	524.8	63.8	2.72	0.205	4.52	0.019
	SD	0.037	181.3	23.5	1.12	0.067	1.45	0.044
PZ6	mean	0.019	374.5	76.5	1.96	0.163	1.36	0.008
	SD	0.020	175.0	34.4	0.79	0.078	0.75	0.009
PZ 7	mean	0.047	293.7	48.8	1.11	0.159	2.37	0.016
	SD	0.075	106.1	21.65	0.86	0.044	0.81	0.038
PZ8	mean	0.022	8.9	1.09	0.138	0.097	0.14	<LQ
	SD	0.004	4.8	0.39	0.019	0.023	0.02	
PZ 9	mean	0.045	1.6	0.100	0.010	0.065	0.28	1.01
	SD	0.038	1.5	0.103	0.009	0.035	0.25	1.11
PZ 10	mean	0.010	2.2	0.083	0.039	0.116	0.20	0.010
	SD	0.014	1.4	0.052	0.017	0.032	0.22	0.012
PZ 11	mean	0.013	5.9	0.412	0.143	0.146	0.12	<LQ
	SD	0.002	2.1	0.248	0.063	0.046	0.11	
PZ 12	mean	0.376	68.1	3.23	0.125	0.052	2.47	2.47
	SD	0.407	149.1	8.10	0.184	0.080	1.45	2.66
Guidelines		0.01	3	0.003	0.01	0.07	0.4	—

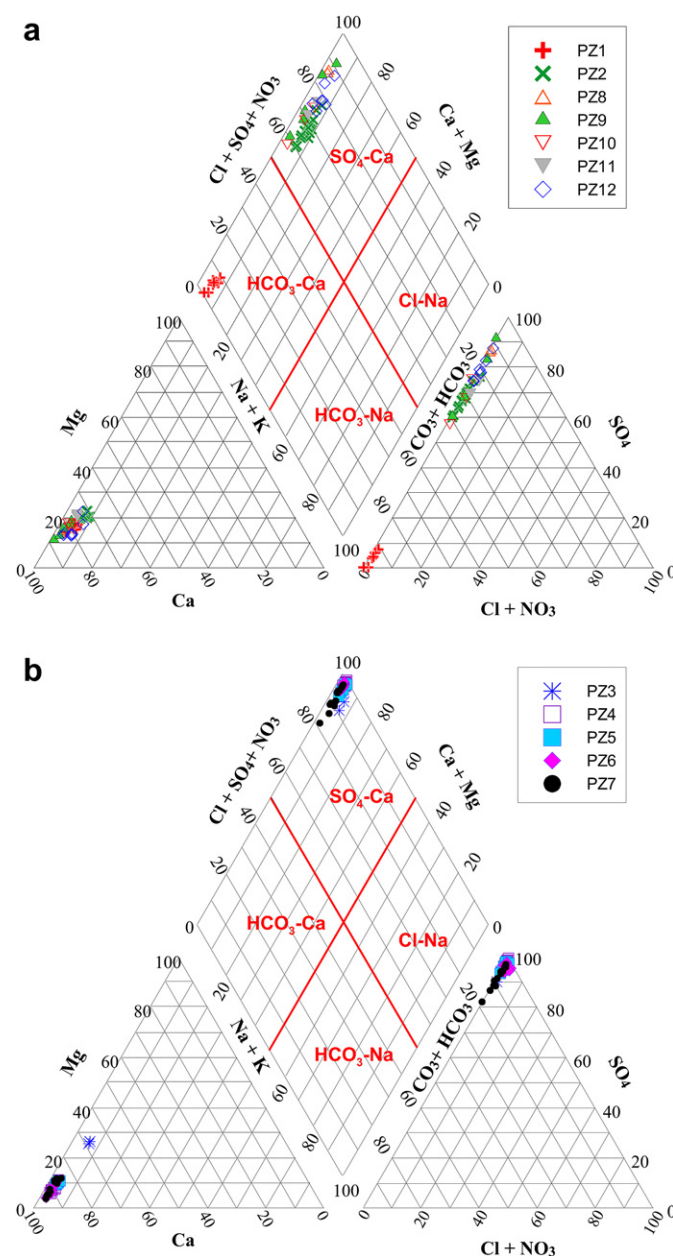


Fig. 4. Data plotted on a Piper Diagram (top: PZ1, PZ2, PZ8 to PZ12; bottom: PZ3 to PZ7).

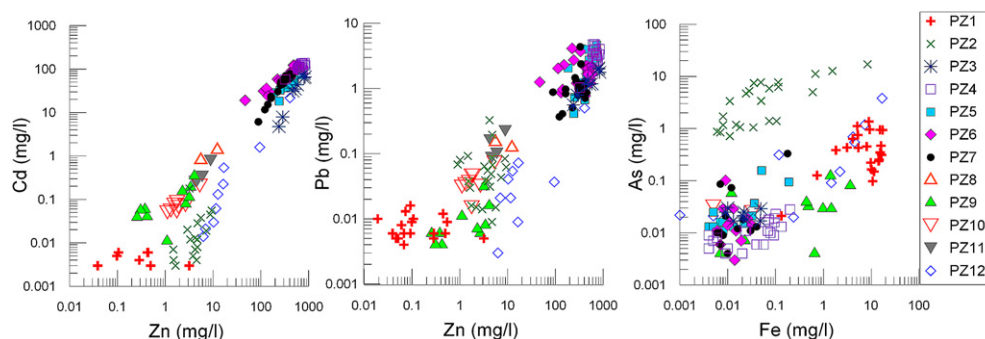


Fig. 5. Aqueous concentrations in the 12 wells (log-scale) for Cd vs. Zn (left); Pb vs. Zn (middle); As vs. Fe (right).

can, however, provide answers concerning processes and possible explanations for field observations.

3.4.1. PZ1 and PZ2 simulations

For the PZ1 simulation (Fig. 6), pyrite was oxidized for Eh > -0.18 V. From -0.18 to -0.1 V, Fe was controlled by siderite (FeCO_3), which allows high aqueous Fe concentrations of up to 6 mg/L in the range of the concentrations observed on site (0.5 – 10 mg/L). Assuming equilibrium with calcite and pH at 6.7, the calculated dissolved inorganic carbon, expressed as HCO_3^- , was 1.3 g L^{-1} , which is in the range of observed values (Table 5). From Eh > -0.12 V, Fe was controlled by hematite with a solubility decreasing to $55 \text{ } \mu\text{g/L}$ at 0 V.

From Eh > -0.13 V, sphalerite was dissolved and aqueous Zn was controlled by $\text{ZnCO}_3 \cdot \text{H}_2\text{O}$, with a solubility of 10.9 mg/L . Galena and CdS released Pb ($27 \text{ } \mu\text{g/L}$) and Cd ($78 \text{ } \mu\text{g/L}$), respectively, for Eh > -0.1 V, and aqueous concentrations were controlled by cerussite (PbCO_3) and otavite (CdCO_3).

For the PZ2 simulation, the reaction pathway was similar but due to a higher fixed pH (7.2) and assuming equilibrium with calcite, the overall HCO_3^- concentration was lower (683 mg L^{-1}), which is in the range of observed values (Table 5). Sulfides were oxidized for lower Eh than in the PZ1 simulation, pyrite was oxidized from Eh > -0.21 V, and sphalerite, galena and CdS at around -0.15 V (Fig. 6). Since the pH was higher, secondary carbonate minerals were less soluble (Zn 5.8 mg L^{-1} , Pb $25 \text{ } \mu\text{g L}^{-1}$, Cd $39 \text{ } \mu\text{g L}^{-1}$ for Eh > -0.12 V). Fe was controlled by hematite but less soluble than for PZ1 simulation, around $1 \text{ } \mu\text{g L}^{-1}$ at 0 V.

In both simulations, for Eh ranging from -0.18 to -0.1 V, the SO_4^{2-} concentration increased rapidly (from 0.1 mg/L to 1.25 g/L) due to sulfide oxidation.

These simulations show that pyrite is the most oxidized sulfide, oxidized before CdS, ZnS or PbS. In PZ1, Fe is assumed to be controlled by siderite, which allowed high concentrations, while Zn, Pb and Cd concentrations were low. PZ2 contained SO_4^{2-} , Zn, Pb and

Cd in greater quantity than PZ1, up to 1000 mg/L for SO_4^{2-} , indicating that sulfide oxidation was more intensive in this area, releasing metals in greater quantities than in PZ1. However, Fe was less soluble, because it might be controlled by oxide precipitation. Both PZ1 and PZ2 simulations and on site observations show that a slight change in reducing conditions leads to a great variability of aqueous sulfate concentrations. Geochemical simulations adequately explain the differences in contamination levels observed in these two wells. Although the wells are side by side, the low sediment permeability in this zone might explain these differences.

3.4.2. PZ4 simulation

In the PZ4 simulation (Fig. 7), due to the fixed Eh (0.3 V), all the initial sulfide minerals were oxidized. The total calculated aqueous carbonate concentration was 56 mg L^{-1} at pH 6, which is within the range of values observed in PZ4 to PZ6 (Table 5). Here, acidity is not buffered by carbonates because the waters have low inorganic carbon concentrations. Fe has a low solubility and is controlled by hematite, which was defined as a secondary mineral in the model. Aqueous SO_4^{2-} depends on the quantity of sulfides oxidized and is controlled by gypsum precipitation for a SO_4^{2-} concentration of up to 2.2 g L^{-1} . Pb is controlled by anglesite (PbSO_4) as previously observed (XRD), with a solubility of around 3.9 mg/L for a pH below 6.

Zn and Cd solubility are controlled by carbonates that are extremely soluble at acidic pH. Zn is highly soluble in acidic water (up to 653 mg L^{-1} for pH < 6) and is controlled by the quantity of Zn released from sphalerite oxidation. For pH > 6.1 , Zn is controlled by $\text{ZnCO}_3 \cdot \text{H}_2\text{O}$. Beyond pH 5.6, Cd is controlled by otavite, which is highly soluble (Cd 106 mg L^{-1}). Finally, Zn, Pb, Cd solubility decreases rapidly with increasing pH, e.g. Cd at 6.8 mg L^{-1} for pH 6.2.

Speciation calculations done with PHREEQC for measured water compositions showed that the waters from PZ8 to PZ11 are in equilibrium with respect to carbonate minerals (calcite, cerussite, otavite and $\text{ZnCO}_3 \cdot \text{H}_2\text{O}$) and gypsum or under-saturated with respect to secondary minerals (Anglesite). Several analyses showed

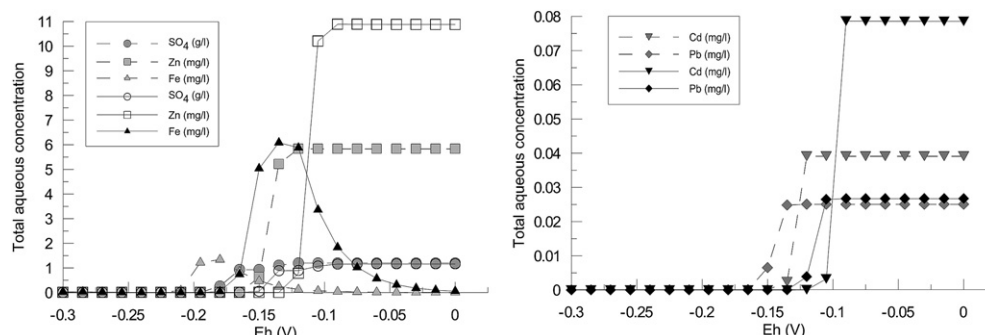


Fig. 6. Simulations of PZ1 and PZ2: solubility of Zn, Fe and SO_4^{2-} (left); Pb and Cd (right) (solid lines: simulation PZ1, pH at 6.7; dashed lines: simulation PZ2 pH at 7.2).

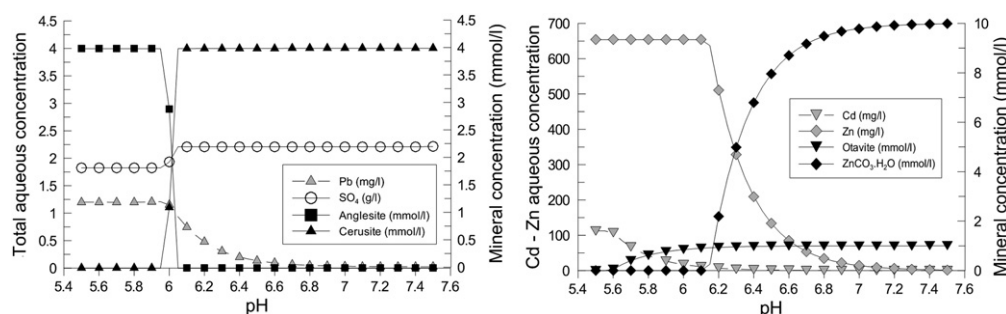


Fig. 7. Simulation of PZ4: solubility of Pb and SO_4^{2-} (left) and Zn and Cd (right) (Eh at 0.3 V).

that waters are in equilibrium or super-saturated with respect to pyromorphite (lead phosphates) (Lions, 2004). Furthermore, in this zone, aqueous metals decrease along the water pathway, probably due to precipitation and adsorption onto clay and organic matter.

4. Discussion

The study highlighted a major mobilization of arsenic and metals in the dredged sediments. It is, therefore, important that the mechanisms involved be understood so that the risk entailed for groundwater can be assessed and remediation strategies proposed for the management of this old deposit.

4.1. Geochemical behavior

Reduced sediments commonly become oxidized when they are exposed to air by dredging and disposal on land. Oxidative processes are known to increase contaminant availability. This study showed how metal and arsenic mobility can vary significantly within a given site with a limited surface area (6 ha).

In Zone 1, the sediments are weakly permeable and hard to aerate, which results in the persistence of anoxic conditions, even 30 years after deposition. Fe and As were readily available in this zone, which might be explained by the release of arsenic usually associated with the release of Fe from sulfides and the relative lack of scavengers, like iron-hydroxides under oxic conditions, able to adsorb arsenic (Plant et al., 2005).

Although a significant correlation between Fe and As was observed in all the waters over time, PZ2 waters could be distinguished as they contain high concentrations of As but relatively low Fe concentrations. Physicochemical characteristics around PZ2 might modify As behavior. High pH values like those measured in PZ2 (up to 7.8) might decrease the sorption of arsenate without any concomitant dissolution of iron oxy-hydroxide (Raven et al., 1998; Bose and Sharma, 2002).

In Zone 2, the oxidation of a large amount of sulfide minerals (up to 10%) and the presence of more acidic waters ($\text{pH} < 6$) and high metal concentrations are similar to those associated with acid mine drainage (Blowes et al., 2003). Oxidizing conditions induce sulfide oxidation, which releases protons, sulfates and metals to the groundwater, while Fe precipitates as oxy-hydroxides and As is removed from solution by adsorption or precipitation (Hartley and Dickinson, 2010). The high metal concentrations measured in Zone 2 waters are similar to those observed in spring water draining mines (Concas et al., 2006).

In the present study, simulated aqueous values are in the range of the very high values measured in the field and metal mobility could be explained by taking into account mineral solubility alone. Organic complexation or pseudo-solubility as colloids were not necessarily the main processes involved here, even if Pb mobilization is rarely observed and generally enhanced by organic matter or

colloids (Jordan et al., 1997). Under oxidizing conditions, simulations suggest a control of Fe in solution by oxide phases such as hematite, as defined in the model. In the field, we would expect that more soluble amorphous hydrated iron oxides precipitate.

4.2. Implications for long-term mobility

These results have implications for long-term mobility at the disposal site scale. During their transition from anoxic to oxic phases, heavy metals that were initially present in insoluble forms became progressively more soluble and mobile. In the site studied here, a large but unquantified stock of initial sulfides remained in the sediment even in the most weathered material (Bataillard et al., 2008). We might expect that dissolved metals in the top layer migrate downward but precipitate or are adsorbed onto minerals or organic phases in the underlying layers under favorable conditions (pH and redox buffering). This might explain why groundwater monitoring showed no impact of the disposal site on the regional aquifer about 9 m below the site (Lions, 2004). Though metals have been immobilized in the layers underlying the source of contaminants, we can not exclude their future re-mobilization. Stigliani (1991) defined the concept of chemical time bombs as “a chain of events resulting in the delayed and sudden occurrence of harmful effects due to the mobilization of chemicals stored in soils and sediments in response to slow alterations in environmental conditions”. We found no evidence of harmful effects, but due to the huge amount of contaminants stored in the disposal site, we strongly advise that precautionary measures be taken to avoid long-term release of toxic chemicals.

In addition, adsorbed metals could be mobilized if the pH dropped or due to surface site ion competition, for example with Ca^{2+} (Lions et al., 2007). Moreover, adsorbed arsenic and metals could be transported by Fe (hydr)oxides, or organic matter as colloids can increase contaminant mobility (Jordan et al., 1997; Slowey et al., 2007; Wang and Mulligan, 2009). Colloid migration might be decreased by porous filtration in the present site due to its low permeability layer as indicated by the presence of perched aquifers. At present, the groundwater in the major aquifer below the site exhibits no colloid contamination.

Remediation strategies will have to take all these factors into consideration in order to avoid any harmful evolution. The geochemical modeling done in this study was a helpful tool to test the processes involved. Further work should involve implementing a reactive transport model for predictive modeling.

5. Conclusion

The study of a dredged-sediment disposal site, heavily contaminated by metals and arsenic, showed that even 30 years after deposition, contaminants were still present mainly as sulfides and that metal and arsenic mobility could vary significantly

depending on the physicochemical conditions within the deposit. Geochemical modeling showed that metal availability is controlled by the sulfide oxidation pathway and carbonate or iron oxide precipitation is directly controlled by redox potential, pH and carbonate content.

In the hydromorphic area of the site, waters were contaminated with As and Fe, while in another area under more oxidizing conditions the consequences of weathering and surface oxidation of sulfides on the mobility of metals such as Zn, Cd or Pb were observed.

No impact on the regional aquifer has yet been observed, probably due to an immobilization of metals and arsenic in the layers underlying the deposited sediments. Nevertheless, this immobilization might be reversible and the present disposal site might represent an environmental hazard. Remediation work should aim to limit infiltration in order to prevent long-term aquifer contamination.

References

- Bataillard, P., Girondelot, B., Guérin, V., Laboudigue, A., Lions, J., van der Lee, J., 2008. Dynamique des éléments traces dans un anthroposol développé sur des sédiments de curage fortement contaminés. I. Migration à l'échelle du profil. *Etude et Gestion des Sols* 15, 7–18.
- Blowes, D.W., Ptacek, C.J., Jambor, J.L., Weisener, C.G., 2003. The geochemistry of acid mine drainage. In: Drever, J.I. (Ed.), *Treatise on Geochemistry. Surface and Ground Water, Weathering and Soils*, vol. 5. Elsevier-Pergamon, Oxford, pp. 149–204.
- Bose, P., Sharma, A., 2002. Role of iron in controlling speciation and mobilization of arsenic in subsurface environment. *Water Research* 36, 4916–4926.
- Bourg, A.C.M., Darmendrail, D., Ricour, J., 1989. Geochemical filtration of riverbank and migration of heavy metals between the Deûle River and the Ansereuilles Alluvion-chalk aquifer (Nord, France). *Geoderma* 44, 229–244.
- Calmano, W., Hong, J., Förstner, U., 1993. Binding and mobilization of heavy metals in contaminated sediments affected by pH and redox potential. *Water Science and Technology* 28, 223–235.
- Cauwenberg, P., Maes, A., 1997. Influence of oxidation on sequential chemical extraction of dredged river sludge. *International Journal of Environment Analytical Chemistry* 68, 47–57.
- Christensen, T.H., 1984. Cadmium soil sorption at low concentration: effect of time, cadmium loading, pH and calcium. *Water, Air and Soil Pollution* 21, 105–114.
- Concas, A., Ardau, C., Cristini, A., Zuddas, P., Cao, G., 2006. Mobility of heavy metals from tailings to stream waters in a mining activity contaminated site. *Chemosphere* 63, 244–253.
- Darmendrail, D., Baize, D., Barbier, P., Freyssinet, P., Mouvet, C., 2000. *Fond géochimique naturel, Etat des connaissances à l'échelle nationale*. Brgm report RP-50518-Fr. Orleans, France.
- Du Laing, G., Rinklebe, J., Vandecasteele, B., Meers, E., Tack, F.M.G., 2009. Trace metal behaviour in estuarine and riverine floodplain soils and sediments: a review. *Science of the Total Environment* 407, 3972–3985.
- Gabler, H.E., 1997. Mobility of heavy metal as function of pH of samples from an overbank sediment profile contaminated by mining activities. *Journal of Geochemical Exploration* 58, 185–194.
- Hartley, W., Dickinson, N.M., 2010. Exposure of an anoxic and contaminated canal sediment: mobility of metal(loid)s. *Environmental Pollution* 158, 649–657.
- Jordan, R.N., Yonge, D.R., Hathhorn, W.E., 1997. Enhanced mobility of Pb in the presence of dissolved natural organic matter. *Journal of Contaminant Hydrology* 29, 59–80.
- King, R.F., Royle, A., Putwain, P.D., Dickinson, N.M., 2006. Changing contaminant mobility in a dredged canal sediment during a three-year phytoremediation trial. *Environmental Pollution* 143, 318–326.
- Lions, J., Van Der Lee, J., Guérin, V., Bataillard, P., Laboudigue, A., 2007. Zinc and cadmium mobility in a 5-year old dredged sediment deposit: experiments and modeling. *Journal of Soils and Sediments* 7, 207–215.
- Lions, J., 2004. *Etude hydrogéochimique de la mobilité de polluants inorganiques dans des sédiments de curage mis en dépôts: expérimentations, étude in situ et modélisations*. PhD thesis, Ecole Nationale Supérieure des Mines de Paris, France, 248 pp.
- Plant, J.A., Kinniburgh, D.G., Smedley, P.L., Fordyce, F.M., Klinck, B.A., 2005. Arsenic and selenium. In: Lollar, B.S. (Ed.), *Treatise on Geochemistry. Environmental Geochemistry*, vol. 9. Elsevier-Pergamon, Oxford, pp. 17–66.
- Raven, K.P., Jain, A., Loeppert, R.H., 1998. Arsenite and arsenate adsorption on ferrihydrite: kinetics, equilibrium, and adsorption envelopes. *Environmental Science & Technology* 32, 344–349.
- Slowey, A.J., Johnson, S.B., Newville, M., Brown, G.E., 2007. Speciation and colloid transport of arsenic from mine tailings. *Applied Geochemistry* 22, 1884–1898.
- Stigliani, W.M., 1991. *Chemical Time Bombs: Definition, Concepts, and Examples*. Executive Rept 16. Intern. Inst. For Applied Systems Analysis, Laxenburg, Austria, p. 23.
- Tack, F.M.G., Callewaert, O.W.J.J., Verloo, M.G., 1996. Metal solubility as a function of pH in a contaminated dredged sediment affected by oxidation. *Environmental Pollution* 91, 199–208.
- Vallee, K., 1999. *Le nickel dans les eaux alimentaires. Application à des champs captants du bassin Artois-Picardie*. PhD, EUDIL, Université de Lille I, Lille, France, 268 pp.
- Van der Lee, J., 1998. *Thermodynamic and Mathematical Concepts of Chess*. Technical Report Nr. LHM/RD/98/39. Ecole des Mines de Paris, Fontainebleau, France.
- Wang, S.L., Mulligan, C.N., 2009. Enhanced mobilization of arsenic and heavy metals from mine tailings by humic acid. *Chemosphere* 74, 274–279.
- Wang, W.Z., Brusseau, M.L., Artiola, J.F., 1997. The use of calcium to facilitate desorption and removal of cadmium and nickel in subsurface soils. *Journal of Contaminant Hydrology* 25, 325–336.